Bioconjugate Chemistry

Article

Cite This: Bioconjugate Chem. 2019, 30, 111−123

pubs.acs.org/bc

Carbon Nitride Dots: A Selective Bioimaging Nanomaterial

Piumi Y. Liyanage,[†] Regina M. Graham,[‡] Raja R. Pandey,[∥] Charles C. Chusuei,[∥] Keenan J. Mintz,[†] Yiqun Zhou,[†] James K. Harper,[§] Wei Wu,[⊥] Athula H. Wikramanayake,[⊥] Steven Vanni,[‡] and Roger M. Leblanc*[,†]

[†]Department of Chemistry, University of Miami, 1301 Memorial Drive, Coral Gables, Florida 33146, United States

[‡]Department of Neurological surgery, Miller School of Medicine, University of Miami, Miami, Florida 33136, United States

[∥]Department of Chemistry, Middle Tennessee State University, Murfreesboro, Tennessee 37132, United States

[§]Department of Chemistry, University of Central Florida, 4111 Libra Drive, Orlando, Florida 32816, United States

[⊥]Department of Biology, University of Miami, Coral Gables, Florida 33146, United States

Supporting Information

ABSTRACT: In contrast to the recent immense attention in carbon nitride quantum dots (CNQDs) as a heteroatom-doped carbon quantum dot (CQD), their biomedical applications have not been thoroughly investigated. Targeted cancer therapy is a prominently researched area in the biomedical field. Here, the ability of CNQDs as a selective bioimaging nanomaterial was investigated to assist targeted cancer therapy. CNQDs were first synthesized using four different precursor sets involving urea derivatives, and the characteristics were compared to select the best candidate material for bioapplications. Characterization techniques such as UV−vis, luminescence, X-ray photoelectron spectroscopy, nuclear magnetic resonance spectroscopy, and transmission electron microscopy were used. These CNQDs were analyzed in *in vitro* studies of bioimaging and labeling using pediatric glioma cells (SJGBM2) for possible selective biolabeling and nanodistribution inside the cell membrane. The *in vitro* cellular studies were conducted under long-wavelength emission without the interference of blue autofluorescence. Thus, excitation-dependent emission of CNQDs was proved to be advantageous. Importantly, CNQDs selectively entered SJGBM2 tumor cells, while it did not disperse into normal human embryonic kidney cells (HEK293). The distribution studies in the cell cytoplasm indicated that CNQDs dispersed into lysosomes within approximately 6 h after the incubation. The CNQDs exhibited great potential as a possible nanomaterial in selective bioimaging and drug delivery for targeted cancer therapy.

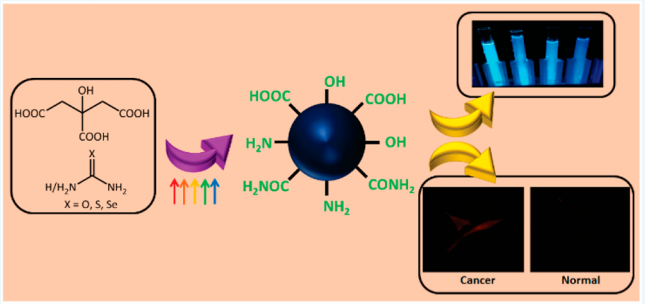

INTRODUCTION

Metal-free quantum dots have attracted great attention in the past decade because of their nontoxic and environmentally friendly features over traditional semiconductor metal quantum dots. The main drawback of traditional semiconductor quantum dots is that they contain toxic heavy metals which leads to adverse health and environmental effects.[1,2] Carbon quantum dots (CQDs) have been one of the promising metal-free materials because of their high photoluminescence, water dispersity, biocompatibility, and nontoxicity.[3−5] Some of the different synthesis methods that have been used are laser ablation,[6,7] electrochemical oxidation,[8] acidic oxidation,[9,10] ultrasonic treatment, and arc discharge.[11,12] In general, these synthesis techniques can be divided into two categories as "top-down" and "bottom-up" procedures. However, many of these CQDs have some problems such as poor luminescent and stability properties because they are known for self-quenching.[13−15]

Alternatively, more research has been focused on heteroatom-doped CQDs to avoid these inherent problems.[12,16,17] Different approaches have been reported to specifically achieve better photoluminescence (PL) for applications in bioimaging.[18,19] For example, near-infrared emission has been achieved through lanthanide hybridization to CQDs.[20] Among these, carbon nitride quantum dots (CNQDs) have gained increasing attention specifically because of their excellent optical properties and structural similarity to graphene. The unique heteroatom structure also enables wide applications because of its functional groups.[21−27]

Carbon nitride has been widely used in sensing, metal detection, catalysis, and solar energy.[28−30] Usually the preparation of carbon nitride has been done with N-rich

Received: October 29, 2018
Revised: December 6, 2018
Published: December 10, 2018

DOI: 10.1021/acs.bioconjchem.8b00784
Bioconjugate Chem. 2019, 30, 111−123

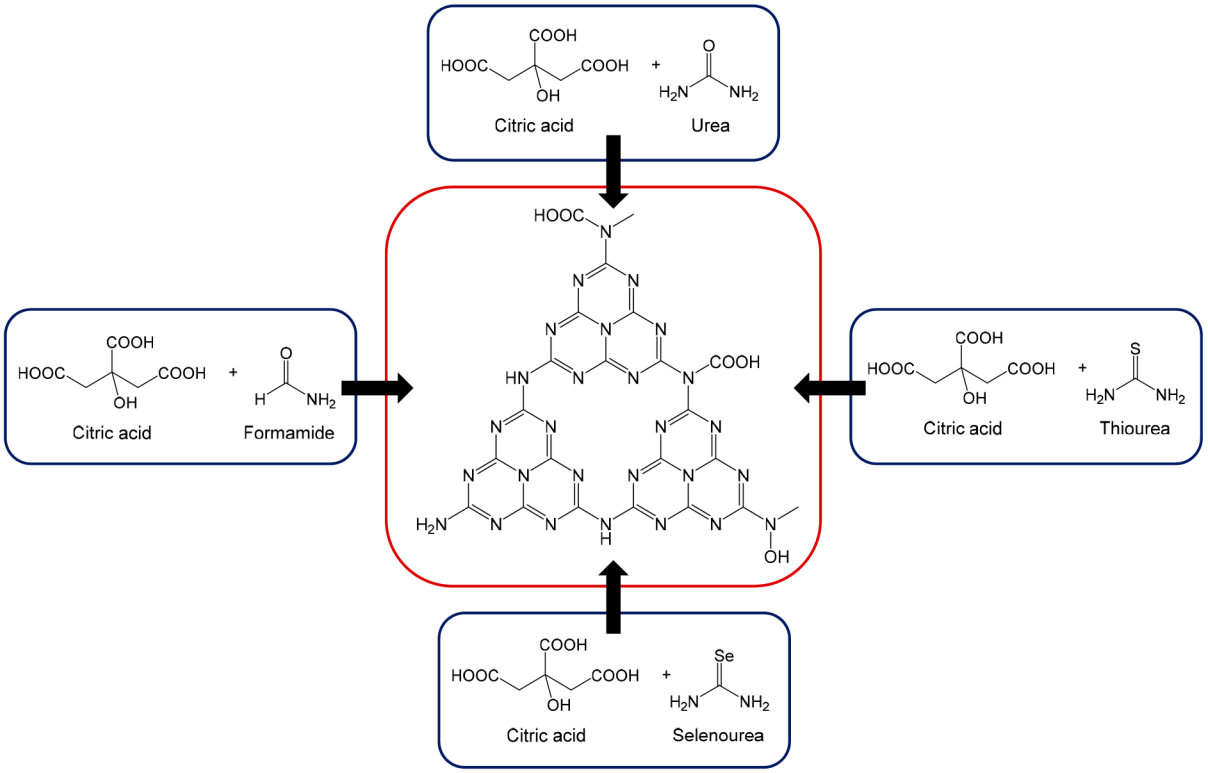

Figure 1. Synthesis of CNQDs with different precursors.

precursors such as melamine, cyanamide, and dicyanamide or from bulk carbon nitride (g-C_3N_4).[28,31]

Various synthetic approaches have been used for these preparations including solvothermal, electrochemical, pyrolysis, and chemical oxidation.[26−28,31,32] However, these syntheses demonstrate some inherent limitations such as the need for high-temperature treatments and specific instrumentation.[27,28] Furthermore, some of the resultant materials consist of large particles thus leading to poor photoluminescent (PL) properties. Because of these concerns, simple synthesis methods are still being investigated. Several research groups have developed different approaches involving different N-precursors. Among those, urea has been a very popular N-rich precursor for CNQD synthesis because of its high abundance and low cost and its high activity under thermal treatment. Zhang et al. used a solid phase thermal treatment and were able to produce a series of g-CNQDs that emit blue to green luminescence by tuning the molar ratio of their two precursors.[21] They report that the fluorescent emission changes significantly from green to blue by increasing the ratio of sodium citrate against urea. Citric acid salts are very popular as a second precursor because of their high abundance of carboxylic groups. Apart from urea, additional syntheses have been reported with other N-precursors such as formamide, ethylenediamine, and thiourea. Barman and Sadhukhan introduced a MAS-II microwave-assisted method with formamide as the sole precursor.[33] A few other reported works are based on amino acids as the N-precursor.[11] The use of amino acids has been inspired mainly because of their biocompatibility. Xiao et al. have reported a one-step microwave-assisted preparation of amino-functionalized CNQDs from chitosan, which is a polysaccharide.[34] Recently these microwave mediated synthesis methods have become more popular due to its fast heating rates over conventional heating techniques as well as the ease of use.[34,35]

So, with these in mind, herein we synthesized strongly luminescent CNQDs using four different urea derivatives as N-precursor in the presence of citric acid (see Figure 1). Among these N-precursors, we report two new syntheses, while urea[36] and thiourea[12,37] have been previously reported as precursors. In this work, the CNQDs from different precursors were compared with respect to characterization and biocompatibility. The CNQDs show excitation-wavelength-dependent emission with significant quantum yields (QY). The efficiency of these metal-free quantum dots in biomedical applications were studied. Interestingly, CNQDs exhibit emission with excitation near 600 nm enabling these to be used for bioimaging without interference from autofluorescence. The nanodistribution of CNQDs in the cell cytoplasm was investigated. Moreover, CNQDs showed that it could serve as a luminescent probe due to its selective targeting ability toward pediatric glioma cells.

RESULTS AND DISCUSSION

Characterization of CNQDs. Carbon nitride nanomaterials are composed primarily of tri-s-triazine rings. Thus, a N-rich precursor was used, in a bottom-up synthesis approach to prepare CNQDs from small molecules. Furthermore, to increase the presence of carboxylic functional groups on the surface of the CNQDs, citric acid was used as the other precursor. Carbon nitride was prepared from four different precursor combinations with different N-precursors alongside citric acid. The N-precursors were urea (U), thiourea (TU), selenourea (SU), and formamide (F). A simple one-step microwave synthesis was used except for citric acid and selenourea synthesis because thermal decomposition of the latter can lead to release of combustion gaseous products. The reaction is a vigorous carbonization upon evaporation of water by heating. Resultant luminescent nanomaterial was purified to

DOI: 10.1021/acs.bioconjchem.8b00784
Bioconjugate Chem. 2019, 30, 111−123

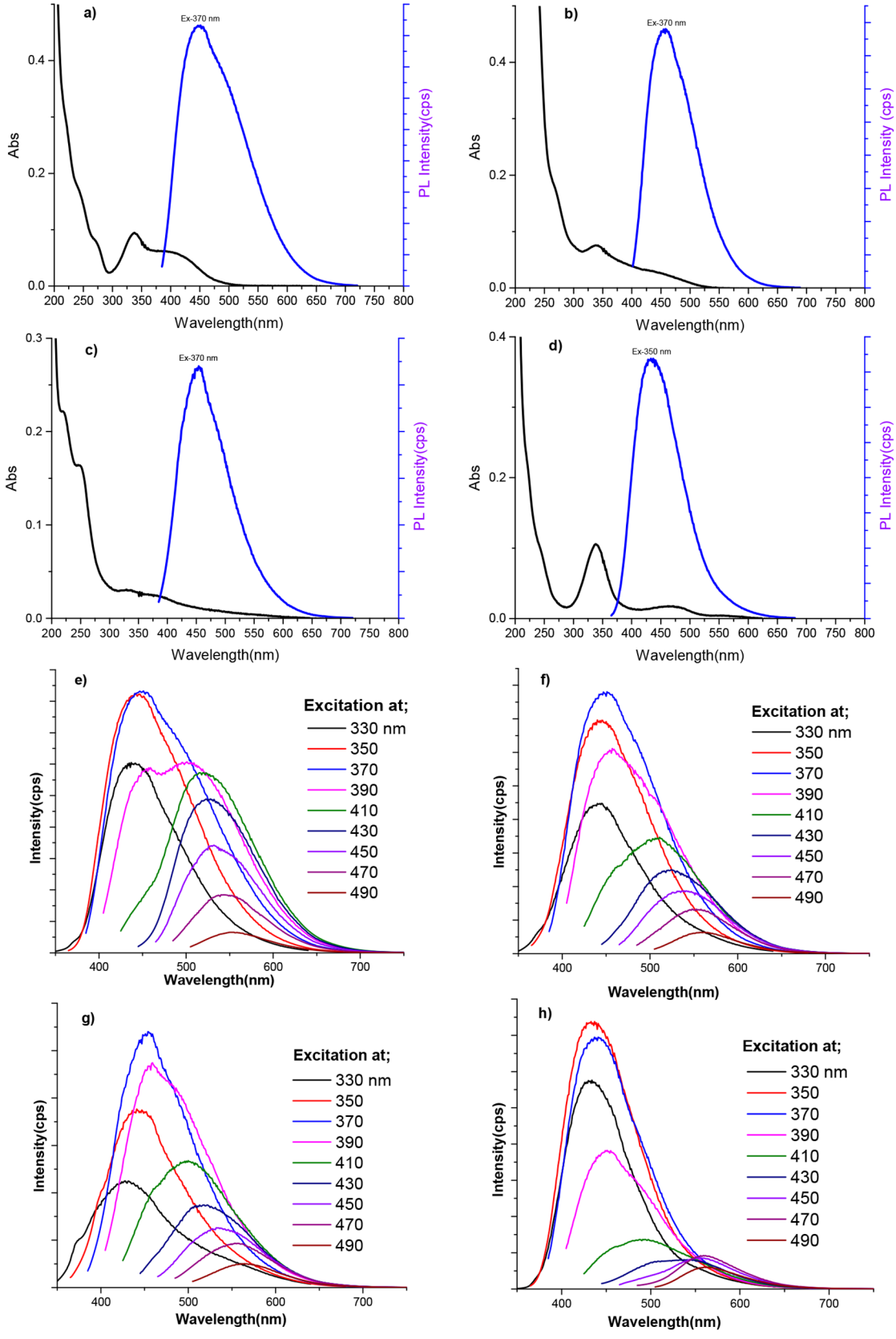

Figure 2. Absorption and emission spectra of CNQDs: (a) CNQD-U, (b) CNQD-TU, (c) CNQD-SU, and (d) CNQD-F. The black line is absorbance and the blue line is maximum emission (Ex: 370 nm). Excitation-dependent fluorescence emission of (e) CNQD-U, (f) CNQD-TU, (g) CNQD-SU, and (h) CNQD-F.

DOI: 10.1021/acs.bioconjchem.8b00784
Bioconjugate Chem. 2019, 30, 111−123

remove any unreacted particles and fragments by filtration and dialysis. The molecular mass of the CNQDs were found to be around 750 Da by MALDI (TOF) mass spectrometry. Thus, a 100−500 Da molecular weight cutoff dialysis membrane was used for the purification. UV−vis absorption, fluorescence, X-ray photoelectron spectroscopy (XPS), transmission electron microscopy (TEM), and atomic force microscopy (AFM) were utilized to characterize the as-prepared CNQDs. An absorption band is found at about 345 nm in all CNQDs samples although with different absorption intensities, and a weak absorption is present toward higher wavelengths (Figure 2). The different absorption intensities could be arising due to differences in the surface states present from each synthesis. Absorption bands obtained in the range of 200−400 nm are ascribed to n− π^* electronic transition of C═O groups and $\pi-\pi^*$ electronic transition of carbon nitride s-triazine rings.[38,39] Also the ratio of these functional groups present could be different leading to the absorption intensity differences. According to a previous report, the band toward the visible region around 400 nm is also due to the different surface states of CNQDs.[40] It is important to note that this band has red-shifted to 476 nm in CNQD-F sample. This could possibly be due to different energy traps present in different surface states.

The obtained PL spectra correspond to the UV−vis absorption features. All four CNQDs demonstrate the excitation-dependent emission with certain variations. In CNQD-U, the emission spectra exhibit an excitation-independent characteristic around 450 nm, in wavelength range of 330−390 nm with a maximum excitation at 370 nm. Then this emission peak red shifts toward 540 nm. These two distinct peaks are clearly visible in the emission spectrum of excitation wavelength at 390 nm. With a normalized PL intensity spectrum, these effects can be observed clearly (Figure S1). Overall the PL emission can be observed to be red-shifted with increasing excitation wavelength. In CNQD-TU even though this clustering of emission spectra is not pronounced as in previous, the peaks are centered at around emission wavelengths 450 and 540 nm. In contrast, the CNQD-SU shows the common excitation wavelength-dependent property of carbon nitride dots with the increase of excitation wavelength. The maximum emission is at 450 nm with an excitation of 370 nm, and the red shift can be observed with the increase of excitation wavelength with fairly even increments. CNQD-F also follows the same pattern, although the excitation wavelength for maximum emission of 450 nm has blue-shifted to 350 from 370 nm, which was the maximum excitation common to the previous three samples.

QY is one of the main characteristics important for carbon-based quantum dots, considering the various applications[41] in sensing and imaging, specifically in biomedical fields. Over the years, although CQDs have reported high QYs through different doping techniques,[42−44] the QYs of CNQDs reported mostly fall in the range of 20−40%.[11,28,32] Most of the low and often varied QYs reported are likely due to the ambiguous composition and structure resulting from uncontrolled syntheses. In this work, we were able to gain fairly high QYs in comparison to the previous reports. The QYs with the respective CNQD samples are noted in Table 1. The calculated QY values show a gradual decrease along the order U > TU > SU = F. Nitrogen is a known heteroatom that can be used to increase QY in carbon-based nanomaterial. It is also worthwhile to note that the absolute value of the zeta potential of CNQD-TU and CNQD-F surfaces are comparatively lower, indicating a lower repulsive force among the dots (Table 1). This could also lead to the low values of QY due to self-quenching from aggregation. All four types of CNQDs emitted bright blue luminescence, when irradiated under 365 nm UV light.

Table 1. Quantum Yield and Zeta Potential of CNQDs

CNQD sample	quantum yield (%)	zeta potential (mV)
CNQD-U	55	−38.8
CNQD-TU	39	−33.1
CNQD-SU	30	−38.4
CNQD-F	30	−32.2

To determine the structural functional groups in CNQDs, FTIR was carried out in the solid phase using an ATR accessory. All the CNQD samples showed similar characteristic peaks in FTIR except for one distinct peak in CNQD-TU, which lies at 2060 cm^{-1} (Figure 3). According to previous reports, this can be assumed to arise from species containing CN bonds such as melem-related compounds that could derive from decomposition of thiourea.[45] The spectra exhibit several characteristic peaks at around 1630 and 1420 cm^{-1}, which can be assigned to aromatic C═N stretches. The characteristic peak at around 770 cm^{-1} in the fingerprint region can be assigned to the breathing mode of s-triazine rings of carbon nitride.[32] The intense peaks at 1705 and 1660 cm^{-1} are from asymmetric C═O and C═N stretching vibrations, respectively. The peak at 1190 cm^{-1} can be ascribed to −C−O− and C−OH groups on the surface of the CNQDs. The broad peak in between 3000 and 3450 cm^{-1} also can be attributed to stretching vibrations of O−H and N−H groups, confirming the availability of these groups on the surface of the CNQDs. In addition, the small peak at 2790 cm^{-1} of O−H stretching vibrations, confirms the availability of − COOH groups on the surface.

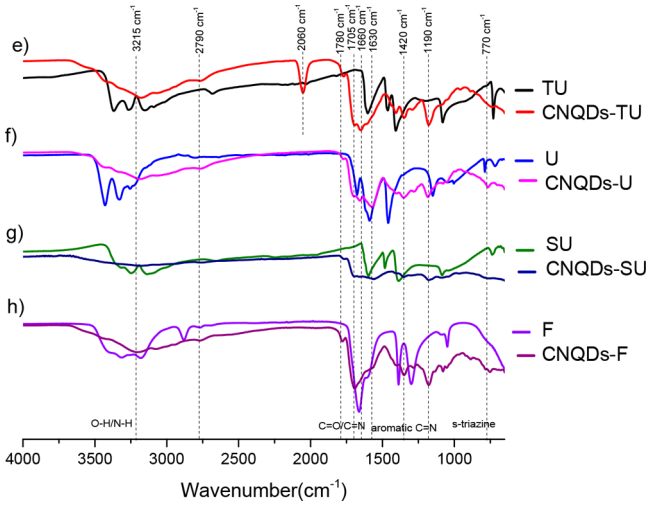

Figure 3. FTIR spectra of CNQDs with the corresponding N-precursors.

To further investigate the surface functional groups, XPS studies were conducted on CNQDs. The results are summarized (Table S1), listing atom % mole fraction composition with fwhm and % deconvoluted peak areas in parentheses. The C 1s binding energy (BE) peak centers at 285.9 and 289.0 eV denote alcohol[37] and carboxylate groups,[46]

DOI: 10.1021/acs.bioconjchem.8b00784
Bioconjugate Chem. 2019, 30, 111−123

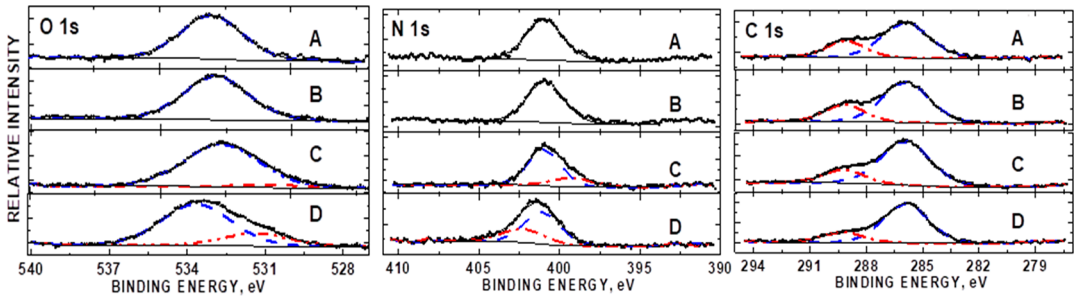

Figure 4. Stack plots of XPS core levels of O 1s, N 1s, and C 1s orbitals of CNQDs: (A) CNQD-U, (B) CNQD-TU, (C) CNQD-SU, and (D) CNQD-F.

respectively, and are common to all of the CNQD samples. These results conform the previous FTIR data obtained.

The N 1s and C 1s core level BEs for CNQD-U and CNQD-TU are identical with respect to each other (Figure 4); however, these BEs differ markedly for the other two with the appearance of additional chemical oxidation states. The deconvoluted C 1s spectra show a gradual increase of C−OH with decrease in −COO− composition within the series from U → TU → SU → F.

The O 1s core levels for CNQD-U and CNQD-TU each show a BE peak center at 533.0 eV from the −C−O− structure.[47−49] CNQD-SU and CNQD-F, on the other hand, show O 1s BE peak centers at 530.9 and ca. 533.5 eV, which is consistent with amide, −COOH,[50] and ether-type O atoms in ester groups,[51] respectively. This result also is consistent with the FTIR C−O peak.

The N 1s BE peak center at 401 eV, observed in all of the CNQD structures, denotes N bound to a graphene lattice (C═N) structure[52] which further confirms the 1670 cm^{-1} FTIR peak. Unique to CNQD-SU not observed in any of the other samples, is the N 1s BE at 399.2 eV, indicative of primary amine N−H[53] and C−N−C[37,54] structures. Unique to CNQD-F is the N 1s BE peak center at 402.2 eV, showing a more electron-density-deficient oxidation state environment as compared with that at 401.0 eV. This result may have been due to the presence of a hyponitrite[55] form in the structure.

Several noteworthy observable trends are summarized in Table 2. Within the series of ureas used in combination with citric acid to form the CNQDs, in the order of U → TU → SU, there is an observable decrease in both the O/C and N/C ratios. Following this same trend, there is an increase in C−OH (at C 1s BE = 285.9 eV) accompanying the decrease of −COO− structure (at C 1s BE = 289.0 eV) as indicated by % deconvoluted peak area ratios of the C 1s core level. Trends in XPS composition coincide with the same order of *ab initio* and density functional theory calculations showing $n_N \rightarrow \pi^*_{[C\text{-}X]}$ (X= O, S, Se) electron delocalization within the series of urea precursors, reported by Bharatam et al.[56] With decreasing O/C, N/C, and C-OH as shown by the deconvoluted XPS peak areas of the C 1s oxidation state within the CNQD structure, there is a direct corresponding increase in the C−N bond rotational barrier, in the order of U < TU < SU. It should be noted that the difference of CNQD-F could be due to its missing NH_2 group in its formula, O═CH(NH_2). It is also worthwhile to note that the C−OH increase along the series could result in some quenching leading to low quantum yields.

Table 2. XPS Composition of CNQDs Prepared

CNQD sample	C−OH	−COO−	O/C	N/C
CNQD-U	72.9%	27.1%	1.12	0.19
CNQD-TU	73.7%	26.4%	0.62	0.16
CNQD-SU	80.1%	19.9%	0.45	0.18
CNQD-F	81.5%	18.4%	0.42	0.02

Solid-state ^{13}C NMR spectra were also studied to confirm the existence of carbon nitride units. The peak centered around 163 ppm can be assigned to the formation of s-triazine structure characteristic to carbon nitride (Figure 5).[32] The omission of this peak in CNQD-TU may be due to greater dynamic motion in the structure which would decrease the effectiveness of the ^1H to ^{13}C short cross-polarization. It is noteworthy to mention that there are no prominent peaks in the region of 110−120 ppm, confirming that there is no formation of graphene-like structures. Furthermore, the peak at around 180 ppm can be assigned to carboxylic acid carbon, again confirming the FTIR results. The resonances at 35 to 43 ppm in all spectra are consistent with the presence of one or more methylene groups on the s-triazine structure (e.g., CH_2−COOH groups in addition to the COOH sites). In addition, in CNQD-U and CNQD-SU, the occurrence of peaks at approximately 35, 43, and 75 ppm are consistent with the presence of unreacted citric acid, perhaps physically adsorbed or encapsulated on the CNQDs. It is notable that the presence of citric acid would not influence the luminescence spectra of the CNQDs as citric acid alone does not fluoresce.

TEM images were studied to understand the surface morphology and *X*−*Y* plane size distribution of the CNQDs (Figure 6). Size histograms were created by considering 100 dots for each CNQD sample. All samples were sonicated for 30 min prior to measurements to breakdown any aggregate formation. Both CNQD-U and CNQD-SU showed a narrow Gaussian size distribution of 1.0−3.8 nm with a mean size of 2.4 nm while CNQD-TU had a wider and asymmetric distribution in range 1.8−7.0 nm with a mean of 4.0 nm, which is almost twice that of the previous two samples. On the other hand, CNQD-F seemed to be less stable and easy to aggregate, which conforms the aggregated clusters shown in TEM image (Figure S2) that are about 20 nm or larger in diameter. AFM was also performed on the CNQDs. AFM images show that the CNQD particles are 2.0−3.5 nm in height, which is consistent with the previous TEM diameter distribution confirming the spherical structure of the CNQDs. Considering the AFM height profile for CNQD-F, which has a distribution of about 5.0 nm (Figure S2), this result suggests that the aggregation is more favorable towards forming flakes (2-D aggregates).

To further understand the surface and the surface charge on the CNQDs created by the different functional groups present,

DOI: 10.1021/acs.bioconjchem.8b00784
Bioconjugate Chem. 2019, 30, 111−123

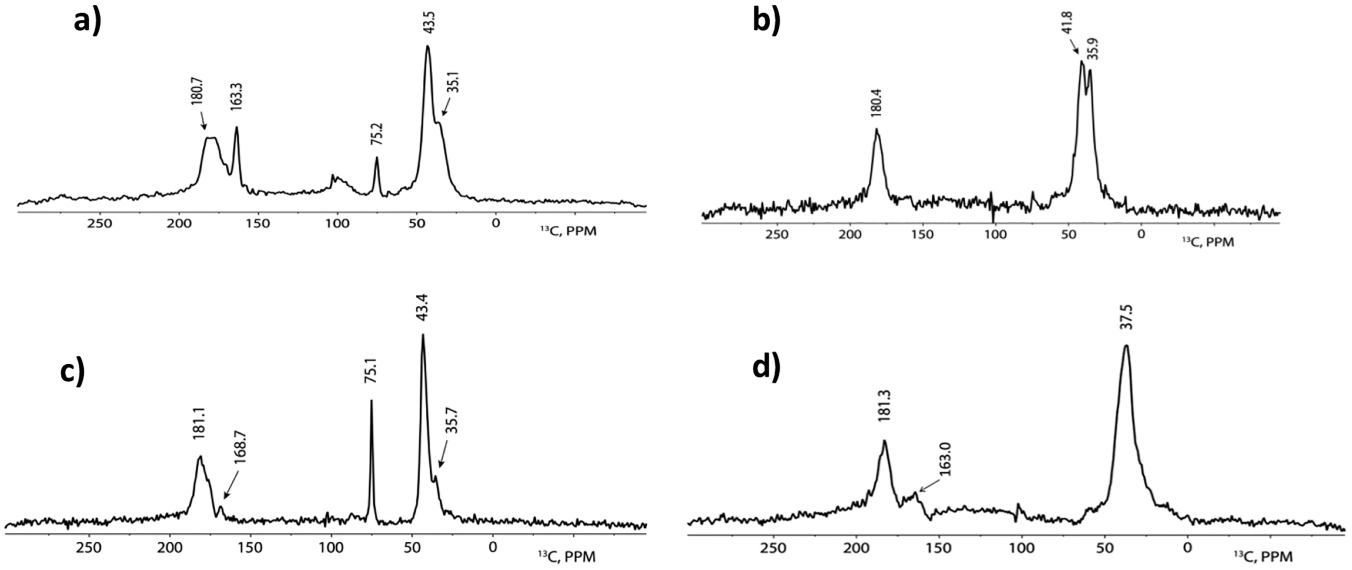

Figure 5. Solid-state ^{13}C NMR spectra for (a) CNQD-U, (b) CNQD-TU, (c) CNQD-SU, and (d) CNQD-F.

the zeta potential measurements were obtained (Table 1). All four samples of CNQDs showed negative potentials. This shows that the dots are composed of negative functional groups such as carboxylic and amide on the surface. The low absolute potentials observed in CNQD-TU and CNQD-F samples can also be confirmed by the TEM images, which shows comparatively higher aggregation with large particle diameters. The highest absolute value of potential was observed in the CNQD-U. This could be attributed to the amount of negative functional groups present on the surface. The highest percentage of −COO− was found in CNQD-U (Table 2).

Cytotoxicity Study. Characteristics such as high QY and PL stability make CNQDs a strong candidate for biomedical applications, especially in bioimaging as luminescent markers. Therefore, viability studies were carried out, to learn about the toxicity and biocompatibility properties of CNQDs. Sea urchin embryos (*purpuratus*) were used for these cytotoxicity evaluations. Sea urchins are a species well-known for acute toxic sensitivity. The development of the embryos was observed, after incubating with CNQDs in seawater for 32 h post fertilization. Concentrations up to 100 μg/mL CNQDs were used. More than 95% of the embryos retained normal development even at these high concentrations (Figure 7). It is worthwhile to note that a concentration as high as 400 μg/mL was possible in the CNQD-SU sample without affecting the embryo development, and more than 95% of embryos were maintained. These results show that the CNQDs have very low acute toxicity toward sea urchin embryos.

***In Vitro* Bioimaging and Cellular Selectivity Studies.** With the above-mentioned PL properties, low cytotoxicity, and good water dispersity, CNQDs can be a good candidate for bioimaging in living cellular organisms. The excitation-dependent emission property is a particular advantage because cells can be imaged in several wavelengths. Living cells and organisms are known to have autofluorescence that emits in blue due to NADPH, proteins, and other amino-functional fluorophores.[57] Thus, bioimaging markers with blue emission are not very effective because the autofluorescence can interfere. In contrast, as-prepared CNQDs have good PL emission even in longer wavelengths, allowing effective and reliable cellular imaging in the red region. In this study, we focused on SJGBM2 glioma cells (pediatric brain tumor), and as a comparison, HEK293 (normal human embryonic kidney) cells were also imaged. Each cell line was treated with 50 μg/mL CNQDs after optimizing different concentrations and incubated for 24 h before imaging under the fluorescent microscope. CNQD-U and CNQD-SU were used for imaging in the cells because of the high QY and low cytotoxicity observed. The dots were observed to have entered the cell cytoplasm and displayed bright PL and did not change the cell shape and viability. The cells were imaged under both blue and red fluorescence (excitation at 358 and 558 nm, respectively) using a fluorescence microscope (Figure 8). Luminescence intensity in the cell nuclei was observed to be lower than that of the cytoplasm confirming that the dots disperse in the cytoplasm more effectively. One possibility of CNQDs entering the cells seems to be through diffusion across the cell membrane owing to the small size of the dots. It is noteworthy that the CNQDs appear to enter the SJGBM2 glioma cells in significant concentrations, but not the normal HEK293 cells. The luminescence in HEK293 cells from CNQDs can be considered negligible considering the autofluorescence of the nontreated cells (Figure 8). This result shows that diffusion is not the main mechanism of CNQDs to cross the cell membrane. Another possible mechanism is that CNQDs could be disguised as glutamine due to their functional groups on the surface. Cancer cells have a high need of metabolic substrates to fulfill their energy and proliferation requirements. Glucose, glutamine, and lactate are the major metabolic substrates for them. During the energy metabolism of cancer cells, a glucose molecule is converted to 2 pyruvates through glycolysis, which eventually produces about 38 molecules of ATP. Lactate is an intermediary of this glycolysis as well as glutaminolysis. It is known that both glycolysis and glutaminolysis support the cancer cell proliferation. However, in oxidative cancer cells, lactate inhibits metabolism of glucose through an allosteric feedback repression.[58] Also cancer cells have several proliferation necessities of glutamine apart from energy metabolism. Glutamine is involved as a nitrogen source for DNA synthesis (glutathione) and in amino acid synthesis (glutamate). Lactate has also been found to upregulate the glutamine transporter expression (ASCT2).[59] From the surface characterizations,

DOI: 10.1021/acs.bioconjchem.8b00784
Bioconjugate Chem. 2019, 30, 111−123

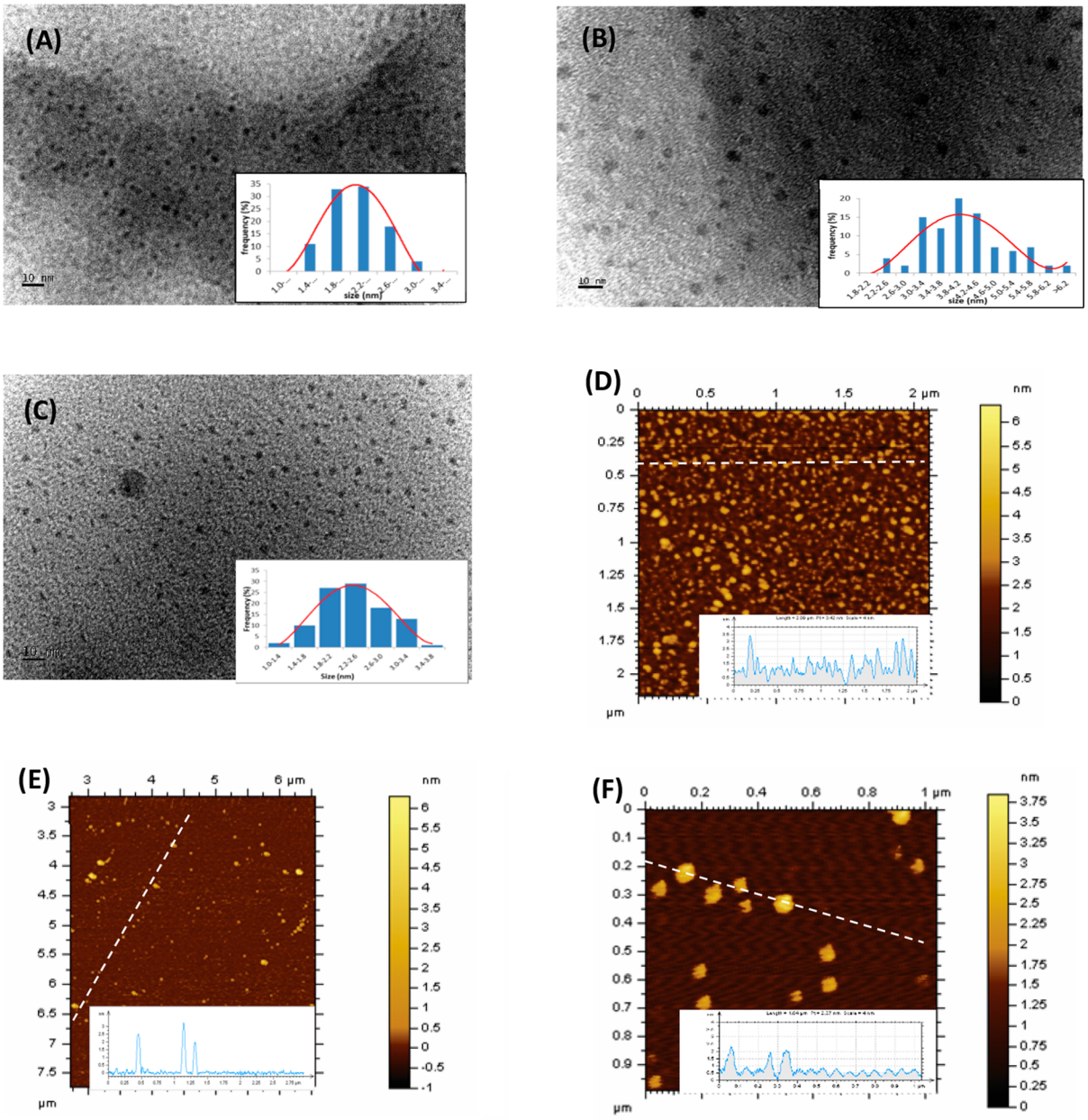

Figure 6. TEM images of CNQDs. (A) CNQD-U, (B) CNQD-TU, and (C) CNQD-SU. The insets show the size histograms. AFM images of (D) CNQD-U, (E) CNQD-TU, and (F) CNQD-SU. The insets show the height profiles.

CNQDs were confirmed to have carboxylic, amide, and amine functional groups which are similar to glutamine. Hence, CNQDs could enter the cancer cells disguised as the metabolic substrate; glutamine, via the ASCT2 transporter. This phenomenon could be a promising approach for tumor identification.

Cancer cells are also known to have high amounts of transferrin (Tf) receptors to facilitate the high O_2 demand. So, the CNQDs were also conjugated with Tf considering the possibility that Tf could more efficiently target cancer cells and would enter in even higher concentrations, owing to the transport means of receptor-mediated endocytosis. CNQD-U was conjugated with Tf through a bioconjugation using EDC/NHS system, and the conjugate was purified and confirmed with UV−vis absorption and fluorescence spectra (Figure S3). The purification process involved using dialysis (3500 Da MW cutoff tube) to remove any unconjugated CNQDs and other small molecules, whereas size-exclusion chromatography (SEC) was conducted to exclude any unconjugated Tf from the conjugate system. The conjugate was also tested for cell viability using three different types of cell lines with a concentration of 1 μM. A cell proliferation assay was conducted for the cell viability studies. The cells were incubated for 48 h, and the cell viability was retained. SJGBM2 cells were treated with 50 μg/mL concentration of Tf-conjugate and incubated for 24 h for imaging. The photoluminescence intensity of the bare CNQDs and the Tf-conjugated CNQDs did not show any significant difference under the fluorescence microscope.

***In Vitro* Distribution Study of CNQDs.** To understand the CNQDs distribution inside the cell cytoplasm, different organelles of SJGBM2 cells were labeled with fluorescent biomarkers. For this study, the early endosomes and lysosomes

DOI: 10.1021/acs.bioconjchem.8b00784
Bioconjugate Chem. 2019, 30, 111−123

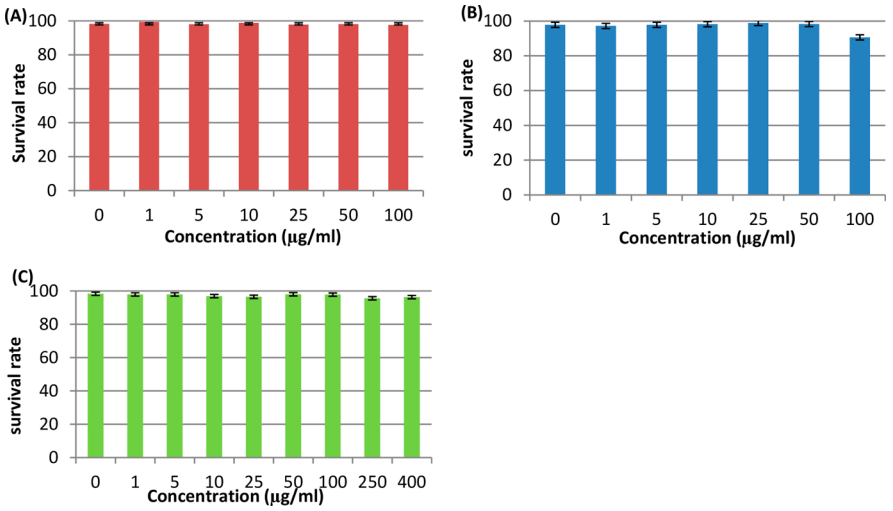

Figure 7. Cytotoxicity studies on sea urchin embryos (A) CNQD-U, (B) CNQD-TU, (C) CNQD-SU.

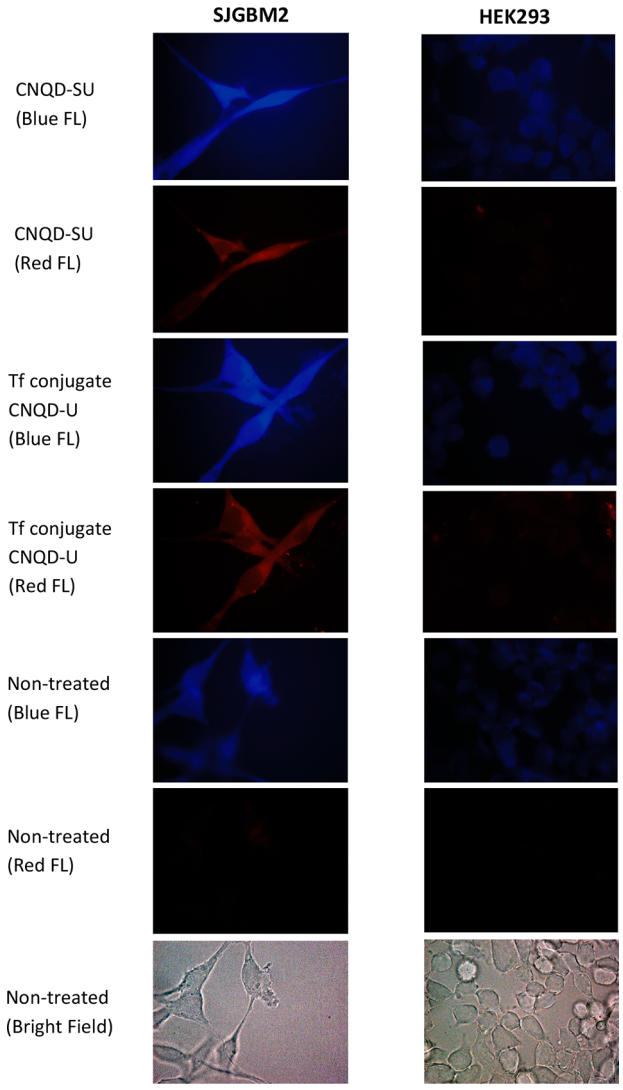

Figure 8. Fluorescence microscopy images of SJGBM2 and HEK293 cells treated with CNQD-SU, Tf-conjugated CNQD. Excitation wavelengths: Blue, 358 nm; Red, 558 nm.

were labeled with a relevant GFP tracker. As previously, the cells were treated with 50 μg/mL CNQDs dispersion and incubated for different time periods as 10 and 30 min; 2, 6, and 24 h. Finally, the fixed cells were imaged under the confocal microscope. As shown in Figure 9, PL accumulation in cells can be seen within the first 10 min, confirming that the cells take up CNQDs quickly. Also, with the luminescence that is observed to be distributed throughout the whole cell, the possibility of CNQDs diffusion through the membrane still stands. Some accumulation is visible in early endosomes within the first 10–30 min, whereas the accumulated bright spots do not overlap with the GFP luminescence of lysosomes. At 2 h, PL accumulation is still prominent in early endosomes and some distribution can be observed in the other parts of the cell. This result shows that CNQDs accumulates in to the early endosomes in less than 2 h and begin moving to other organelles. By 6 h, the CNQDs start to move into lysosomes. In Figure 9, it can be seen that some of the PL spots overlap with the lysosomes, confirming that the CNQDs have moved into lysosomes. At the end of 24 h, the luminescence can be seen mostly accumulated in the lysosomes even though the other parts of the cytoplasm still emit low fluorescence indicating that there could be other organelles that trap CNQDs. Endosomes are membrane bound vesicles that fold inwardly to take up matter from extracellular fluid by endocytosis. The size of these endosome vesicles can vary with the matter that it takes in. Some part of CNQDs uptake probably happens through pinocytosis (one of the primary mechanisms of endocytosis) in which the cell would take-up liquid droplets of extracellular fluid where CNQDs are dispersed in. Lysosomes are cellular organelles which contain enzymes capable of breaking down all types of biological polymers. These function as the digestive system to digest or degrade the matter taken from extracellular fluid and obsolete from inside of the cell. Thus, the dots fused into early endosomes through endocytosis vesicles, gradually mature to late endosomes which transfer to lysosomes which contains the acid hydrolase enzymes. Therefore, CNQDs could be a promising nanocarrier for targeted drug delivery.

CONCLUSIONS

In summary, a CNQD synthesis was developed, and characteristic comparison was performed to understand the best candidate for biomedical applications. Considering the high QY, good stability, low cytotoxicity, and other similar characteristics, CNQD-U and CNQD-SU were used for

DOI: 10.1021/acs.bioconjchem.8b00784
Bioconjugate Chem. 2019, 30, 111–123

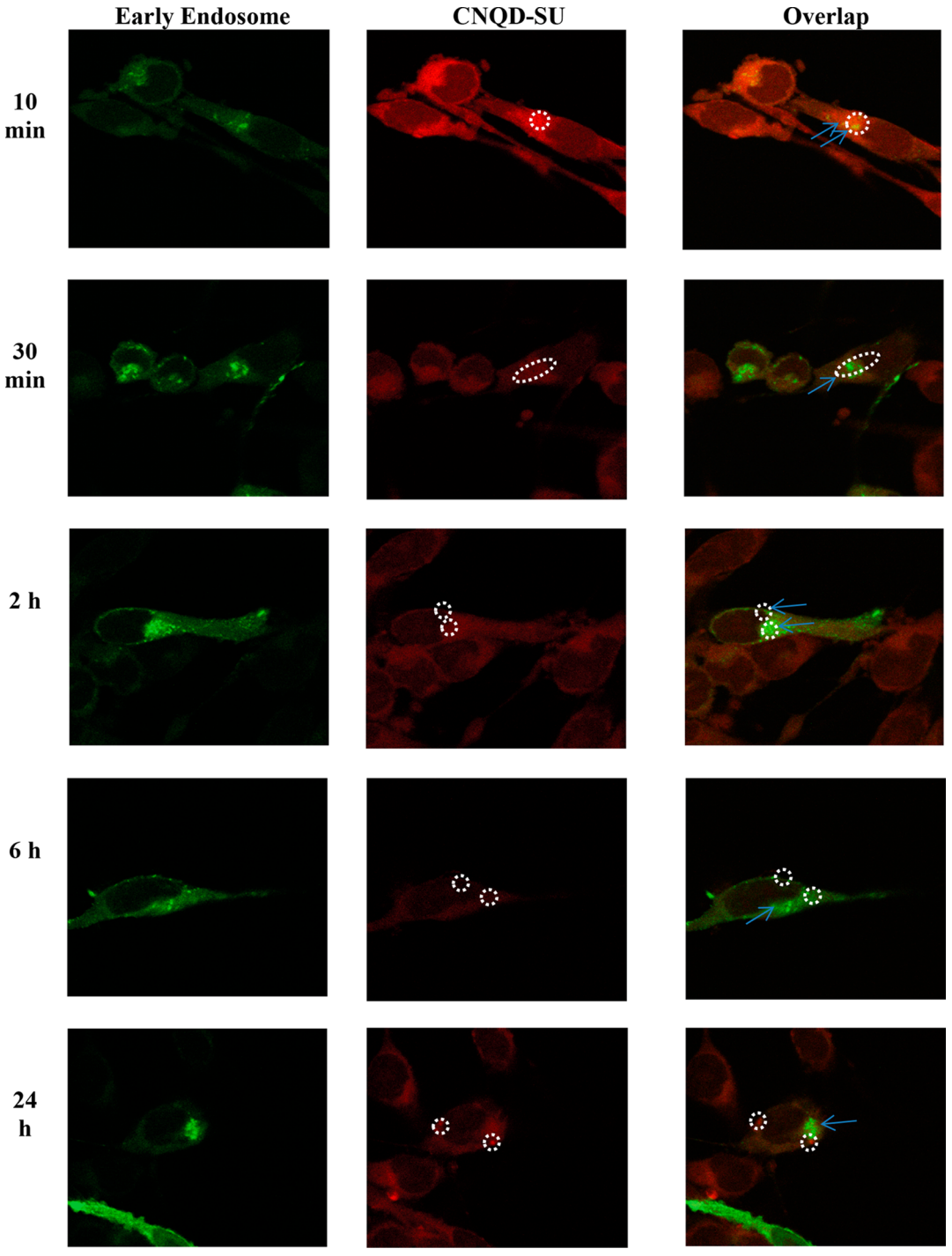

Figure 9. continued

DOI: 10.1021/acs.bioconjchem.8b00784
Bioconjugate Chem. 2019, 30, 111−123

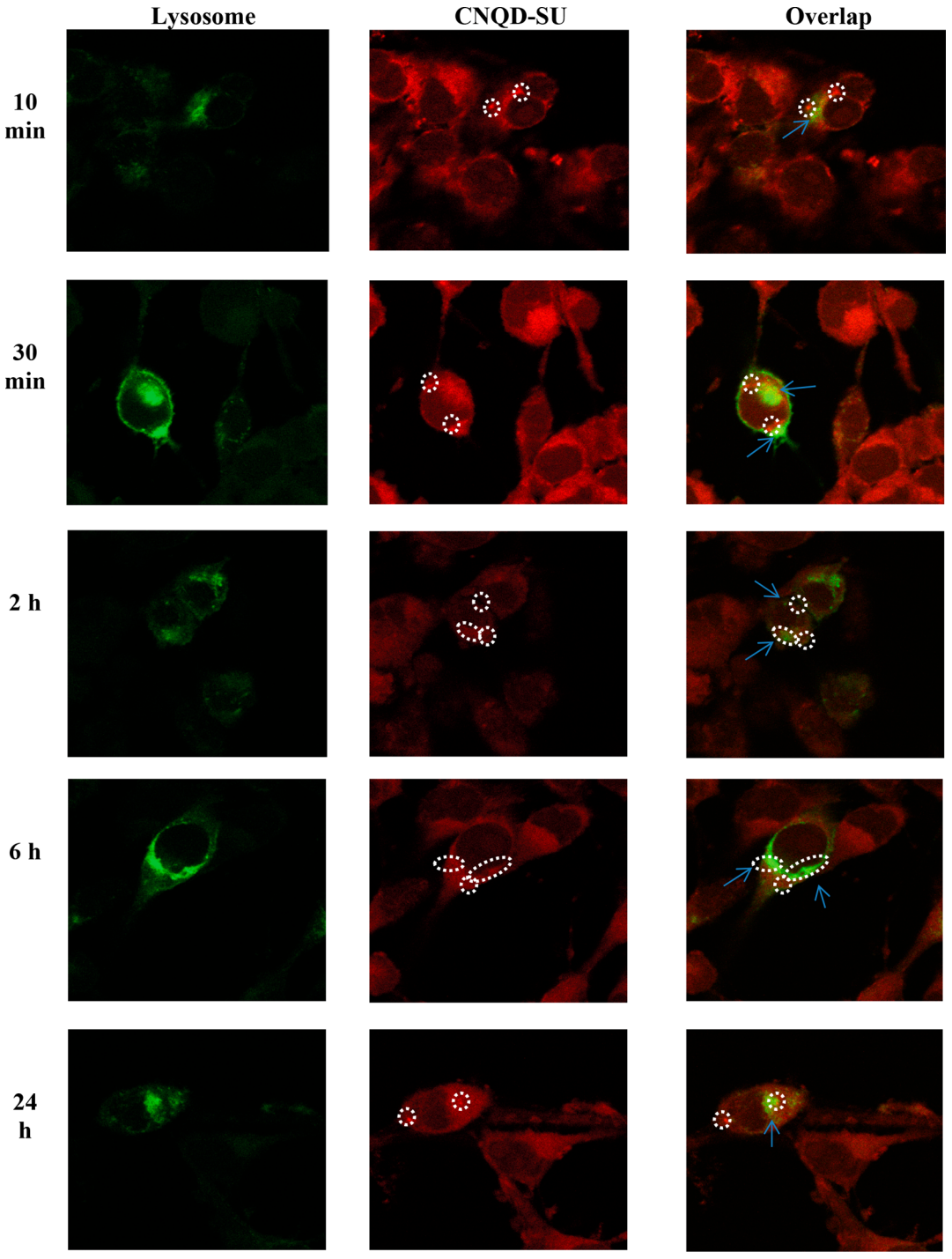

Figure 9. CNQDs distribution in the cell (into early endosomes and lysosomes) with a confocal microscope using a time lapse study. The CNQDs were imaged in red luminescence and both early endosome and lysosome trackers are green fluorescent. The brightest spots of CNQD-SU are labeled in white circles while lysosomes and endosomes are pointed with blue arrows. The third column indicates the overlap of first two images at each time. Excitation wavelengths: Green, 488 nm; Red, 594 nm.

bioimaging applications. The dots were capable of selectively entering the cytoplasm of SJGBM2 tumor cells and emitting bright PL in wavelengths of the red region. This could be an effective labeling technique in tumor identification as well as fluorescence-guided brain surgery, if the nanomaterial could effectively cross the blood-brain barrier and enter the central nervous system. Moreover, the CNQDs were observed to enter the lysosome in about 6 h upon uptake by the cells. This confirms the biodegradability of CNQDs. Also, CNQDs nanomaterial can serve as a promising delivery vehicle for drugs to be released inside the cell by incorporating a pH change inside the lysosome.

EXPERIMENTAL SECTION

Materials Used. Anhydrous citric acid (BDH) was obtained from VWR (West Chester, PA). Urea was acquired from Eastman Kodak Company (NY, U.S.A.). Thiourea (99%) and quinine hemisulfate monohydrate were bought from Alfa

DOI: 10.1021/acs.bioconjchem.8b00784
Bioconjugate Chem. 2019, 30, 111−123

Aesar (Heysham,England). Selenourea (98%) and formamide (99+ %) spectrophotometric grade were purchased from Sigma-Aldrich (St. Louis, MO). Human transferrin (holo) was from MP biomedicals (produced in France). Compressed argon with ultrahigh purity was from Airgas. The deionized water used was purified using a Modulab 2020 water purification system acquired from Continental Water Sys. Corp. (San Antonio, TX). The purified water has a surface tension of 72.6 $mN{\cdot}m^{-1}$, a resistivity of 18 MΩ·cm, and a pH of 6.6 ± 0.3 at 20.0 ± 0.5 °C. All the chemicals were used as received.

Synthesis of the Carbon-Nitride Dots (CNQDs). The CNQDs were synthesized using four different precursor sets. Citric acid was precursor in each set, and the others were urea, thiourea, selenourea, and formamide. The synthesis was a simple hydrothermal microwave-mediated procedure except for the combination involving selenourea for which a normal hydrothermal approach was used.

Citric acid (0.5 g) and urea (0.5 g) were dissolved in 25 mL of deionized water and was stirred vigorously for overnight. Then the mixture was put into a domestic microwave oven of 700 W and was heated for 7 min until all the water evaporates. The resultant black solid remaining at the bottom of the beaker was collected, dispersed in about 15 mL of deionized water and sonicated for 30 min. The dispersion was centrifuged for 15 min at 1500 rpm twice to remove any precipitation. The supernatant was then filtered through a 0.2 μm filter membrane to remove any remaining large particles. Then the filtrate was dialyzed in a 100−500 Da MW cutoff dialysis tubing for 3 days in deionized water; water was changed every 24 h. Finally, the water was evaporated using a rotovap with heating to 70−80 °C. The above same procedure was followed for the precursor sets of citric acid−thiourea and citric acid−formamide.

For citric acid−selenourea, microwave approach was not used due to the possibility of combustion gas release. Citric acid (0.5 g) and selenourea (0.5 g) were dissolved in 25 mL of deionized water and stirred vigorously for overnight. Then the mixture was heated to 180 °C for 4.5 h in a sand bath with continuous stirring and under the protection of argon gas flow. The reaction was conducted in an open flask to facilitate the evaporation of water. After cooling down to room temperature, the flask was kept in argon environment for 48 h. Then the same purification procedure mentioned above was conducted.

Characterization of the CNQDs. The as-prepared CNQDs were characterized by UV−vis absorption in a 1 cm quartz cuvette (Starna Cells) using a Cary 100 UV−vis spectrophotometer (Agilent Technologies) in aqueous medium. Luminescent emission spectra of CNQDs were measured in aqueous solution (1 cm path length quartz cuvette) by a Horiba Jobin Yvon Fluorolog−3 with a slit width of 5 nm for both excitation and emission. The normalization of emission spectra was obtained using normalization function in the OriginPro 9.1 software. The normalized spectra were created with the *y*-axis normalized to 1. The Fourier transformation infrared (FTIR) spectra were recorded using a PerkinElmer Frontier with a universal ATR sampling accessary using air as the background. The mass spectroscopy was done with an ESI Mass Spectrometer (Bruker Microtof-Q). A DLS nano series Malvern Zetasizer was used for the zeta potential measurements. The surface morphologies were obtained with a 5420 Atomic Force Microscope (Agilent Technologies) using tapping mode. Transmission electron microscopy (TEM) was performed using a JEOL 1200X TEM. X-ray photoelectron spectra (XPS) were acquired using a PerkinElmer PHI 560 system with a double-pass cylindrical mirror analyzer operated using a Mg Kα anode with a $h\nu$ = 1253.6 eV photon energy operated at 13 kV and 250 W. Carbon nitride dot samples were mounted as powders onto the sample holder using conductive double-sided tape (Ted Pella, Inc.; Redding, CA, U.S.A.).

Quantum Yield Calculations. The QY (Φ) of as-prepared CNQDs were obtained by comparing the integrated PL intensities and the absorbance values using quinine sulfate as the reference. Quinine sulfate (literature value of Φ_R = 0.60 at an excitation wavelength of 350 nm)[60] dissolved in 0.1 N H_2SO_4 (refractive index, η_R = 1.34) was used for the measurements. CNQDs samples were dissolved in deionized water. Absorbance in the 1 cm path length cuvette was always maintained under 0.05 at the desired excitation wavelength. The QY was calculated using the following equation, eq 1:

$$\Phi_R = \Phi \times \frac{\eta^2}{\eta_R^2} \times \frac{I_R}{I} \times \frac{A}{A_R} \quad (1)$$

where I is the measured integrated PL intensity, η is the refractive index, and A is the absorbance. The reference is denoted with the subscript, R.

Bioconjugation with Transferrin. CNQD-U (8 mg) was dispersed in 3 mL of phosphate buffer solution (PBS) (pH = 7.4) and mixed with a solution of 17 mg of EDC in 1 mL PBS and kept under constant stirring. NHS (13 mg) in 1 mL of PBS was added to the stirring mixture at the half-hour mark, and 2 mg of Tf in 1 mL of PBS at the 1 h mark. Then the mixture was kept stirring overnight, dialyzed for 3 days in a 3500 Da MW cutoff dialysis tubing and further purified through SEC to remove unconjugated Tf. The stationary phase used was Sephacryl S-300. The purified conjugate was lyophilized in to a powder. Conjugation was confirmed using MS MALDI-TOF spectra.

Cytotoxicity Studies of CNQDs to Sea Urchins. Fertilized eggs of sea urchin embryos (*purpuratus*) were plated in a 96-well plate with about 100 eggs per well. The eggs were incubated in different concentrations of CNQDs as 0, 1, 5, 10, 25, 50, 100, 250, 400 μg/mL dispersed in 200 μL of seawater. The plate was incubated at 15 °C. The percentage of survival was calculated at 32 h post fertilization (gastrula stage). Three biological replicates were involved in each.

Cell Culture and Cell Viability Studies with MTS Assay. SJGBM2, CHLA200 (pediatric glioblastoma cell lines) were obtained from the Children's Oncology Group (COG, Lubbock, TX) and U87 (adult glioblastoma cell line), HEK293 (human embryonic kidney cell line) were purchased from the American Type Culture Collection (ATCC, Manassas, VA, U.S.A.). All cell lines were cultured in RPMI-1640 media (ThermoFisher Scientific, Waltham, MA, U.S.A.), supplemented with 10% fetal bovine serum (FBS) and 1% penicillin/streptomycin (both from Gemini Biosciences, West Sacramento, CA), and maintained by incubating at 37 °C in humidified 5% CO_2. Cells were routinely tested for mycoplasma using LookOut mycoplasma PCR detection kit (Sigma-Aldrich, St. Louis, MO) according to the manufacturer's instructions.

Cell viability was determined by using the CellTiter 96 AQueous One Solution Cell Proliferation Assay (MTS) (Promega Madison, WI). Cells were plated in 96-well plates at a density of $0.(5-2) \times 10^4$ cells per well (depending on cell lines) in 100 μL of RPMI supplementary media and incubated

DOI: 10.1021/acs.bioconjchem.8b00784
Bioconjugate Chem. 2019, 30, 111−123

for 24 h. Then cells were treated with 2 μM transferrin conjugate of CNQD-U dispersed in 100 μL RPMI. Viability was determined with MTS assay after 72 h of incubation as per manufacturer instructions. Absorbance was measured at 490 nm using BoiTek Synergy HT plate reader.

***In Vitro* Bioimaging.** SJGBM2 and HEK293 cells were plated in 24-well plates on FBS coated glass coverslips at a density of 1×10^4 in 200 μL RPMI and incubated for 24 h. Then the media was aspirated, and the cells were retreated with 200 μL RPMI solutions containing 50 μg/mL concentrations of CNQD-U, CNQD-SU and transferrin conjugated CNQD-U and incubated for required time periods (10, 30 min, 2, 6, and 24 h). For the distribution studies, 6−8 μL of each GFP tracker (early endosome and lysosome) from Molecular Probes (Eugene, OR) was added to the wells at the time of treatment of CNQDs per instructions of manufacturer. At the end of incubation, cells were washed with PBS twice and fixed with 4% paraformaldehyde for 20 min. The coverslips were mounted on to glass slides before imaging. For fluorescence imaging an Olympus BX51 fluorescence microscope was used. For the distribution studies, an Olympus FV1000 confocal microscope was used.

■ ASSOCIATED CONTENT

Supporting Information

The Supporting Information is available free of charge on the ACS Publications website at DOI: 10.1021/acs.bioconjchem.8b00784.

Normalized fluorescence intensity spectra, XPS elemental atom % and binding energies, CNQD-F characterization - TEM, AFM images and cytotoxicity study, and detailed characterization of Tf conjugate CNQD-U (CNQD-U-Tf) -UV−vis absorption, fluorescence emission, FTIR spectrum, and cytotoxicity (PDF)

■ AUTHOR INFORMATION

Corresponding Author

*E-mail: rml@miami.edu.

ORCID

Roger M. Leblanc: 0000-0001-8836-8042

Notes

The authors declare no competing financial interest.

■ ACKNOWLEDGMENTS

R.L. gratefully acknowledges the support of the National Science Foundation under Grant 011298 and National Institute of Health under Grant 009887. R.G. gratefully acknowledges the support of the Mystic Force Foundation.

■ ABBREVIATIONS

CQDs, carbon quantum dots; CNQDs, carbon nitride quantum dots; PL, photoluminescence; QY, quantum yield; BE, binding energy

■ REFERENCES

(1) Lewinski, N., Colvin, V., and Drezek, R. (2008) Cytotoxicity of nanoparticles. *Small 4*, 26−49.

(2) Derfus, A. M., Chan, W. C. W., and Bhatia, S. N. (2004) Probing the cytotoxicity of semiconductor quantum dots. *Nano Lett. 4*, 11−18.

(3) Esteves da Silva, J. C. G., and Goncalves, H. M. R. (2011) Analytical and bioanalytical applications of carbon dots. *TrAC, Trends Anal. Chem. 30*, 1327−1336.

(4) Luo, P. G., Sahu, S., Yang, S. T., Sonkar, S. K., Wang, J., Wang, H., LeCroy, G. E., Cao, L., and Sun, Y. P. (2013) Carbon quantum dots for optical bioimaging. *J. Mater. Chem. B 1*, 2116−2127.

(5) Li, H., He, X., Kang, Z., Huang, H., Liu, Y., Liu, J., Lian, S., Tsang, C. H. A., Yang, X., and Lee, S. T. (2010) Water-soluble fluorescent carbon quantum dots and photocatalyst design. *Angew. Chem., Int. Ed. 49*, 4430−4434.

(6) Cao, L., Wang, X., Meziani, M. J., Lu, F., Wang, H., Luo, P. G., Lin, Y., Harruff, B. A., Veca, L. M., Murray, D., et al. (2007) Carbon dots for multiphoton bioimaging. *J. Am. Chem. Soc. 129*, 11318−11319.

(7) Sun, Y. P., Zhou, B., Lin, Y., Wang, W., Fernando, K. A. S., Pathak, P., Meziani, M. J., Harruff, B. A., Wang, X., Wang, H., et al. (2006) Quantum-sized carbon dots for bright and colorful photoluminescence. *J. Am. Chem. Soc. 128*, 7756−7757.

(8) Zhang, Y. L., Wang, L., Zhang, H. C., Liu, Y., Wang, H. Y., Kang, Z. H., and Lee, S. T. (2013) Graphitic carbon quantum dots as a fluorescent sensing platform for highly efficient detection of Fe^{3+} ions. *RSC Adv. 3*, 3733−3738.

(9) Tian, L., Ghosh, D., Chen, W., Pradhan, S., Chang, X., and Chen, S. (2009) Nanosized carbon particles from natural gas soot. *Chem. Mater. 21*, 2803−2809.

(10) Shi, W., Wang, Q., Long, Y., Cheng, Z., Chen, S., Zheng, H., and Huang, Y. (2011) Carbon nanodots as peroxidase mimetics and their applications to glucose detection. *Chem. Commun. 47*, 6695−6697.

(11) Niu, W. J., Li, Y., Zhu, R. H., Shan, D., Fan, Y. R., and Zhang, X. J. (2015) Ethylenediamine-assisted hydrothermal synthesis of nitrogen-doped carbon quantum dots as fluorescent probes for sensitive biosensing and bioimaging. *Sens. Actuators, B 218*, 229−236.

(12) Lu, Y. C., Chen, J., Wang, A. J., Bao, N., Feng, J. J., Wang, W., and Shao, L. (2015) Facile synthesis of oxygen and sulfur co-doped graphitic carbon nitride fluorescent quantum dots and their application for mercury(II) detection and bioimaging. *J. Mater. Chem. C 3*, 73−78.

(13) Wu, P., and Yan, X. P. (2013) Doped quantum dots for chemo/biosensing and bioimaging. *Chem. Soc. Rev. 42*, 5489−5521.

(14) Zhou, Y., Sharma, S. K., Peng, Z., and Leblanc, R. M. (2017) Polymers in carbon dots: A review. *Polymers 9*, 67−87.

(15) Zhou, Y., Mintz, K. J., Oztan, C. Y., Hettiarachchi, S. D., Peng, Z., Seven, E. S., Liyanage, P. Y., De La Torre, S., Celik, E., and Leblanc, R. M. (2018) Embedding carbon dots in superabsorbent polymers for additive manufacturing. *Polymers 10*, 921−933.

(16) Sun, D., Ban, R., Zhang, P. H., Wu, G. H., Zhang, J. R., and Zhu, J. J. (2013) Hair fiber as a precursor for synthesizing of sulfur- and nitrogen- co-doped carbon dots with tunable luminescence properties. *Carbon 64*, 424−434.

(17) Chandra, S., Patra, P., Pathan, S. H., Roy, S., Mitra, S., Layek, A., Bhar, R., Pramanik, P., and Goswami, A. (2013) Luminescent S-doped carbon dots: an emergent architecture for multimodal applications. *J. Mater. Chem. B 1*, 2375−2382.

(18) Wu, F., Su, H., Wang, K., Wong, W. K., and Zhu, X. (2017) Facile synthesis of N-rich carbon quantum dots from porphyrins as efficient probes for bioimaging and biosensing in living cells. *Int. J. Nanomed. 12*, 7375−7391.

(19) Su, H., Liao, Y., Wu, F., Sun, X., Liu, H., Wang, K., and Zhu, X. (2018) Cetuximab-conjugated iodine doped carbon dots as a dual fluorescent/CT probe for targeted imaging of lung cancer cells. *Colloids Surf., B 170*, 194−200.

(20) Wu, F., Su, H., Zhu, X., Wang, K., Zhang, Z., and Wong, W. K. (2016) Near-infrared emissive lanthanide hybridized carbon quantum dots for bioimaging applications. *J. Mater. Chem. B 4*, 6366−6372.

(21) Zhang, Y., Liu, J., Wu, G., and Chen, W. (2012) Porous graphitic carbon nitride synthesized via direct polymerization of urea for efficient sunlight-driven photocatalytic hydrogen production. *Nanoscale 4*, 5300−5303.

(22) Zhou, J., Yang, Y., and Zhang, C. Y. (2013) A low-temperature solid-phase method to synthesize highly fluorescent carbon nitride dots with tunable emission. *Chem. Commun. 49*, 8605−8607.

(23) Liu, S., Tian, J., Wang, L., Luo, Y., Zhai, J., and Sun, X. (2011) Preparation of photoluminescent carbon nitride dots from CCl_4 and

DOI: 10.1021/acs.bioconjchem.8b00784
Bioconjugate Chem. 2019, 30, 111−123

1,2-ethylenediamine: a heat-treatment based strategy. *J. Mater. Chem. 21*, 11726−11729.
(24) Liu, S., Wang, L., Tian, J., Zhai, J., Luo, Y., Lu, W., and Sun, X. (2011) Acid-driven, microwave-assisted production of photoluminescent carbon nitride dots from N,N-dimethylformamide. *RSC Adv. 1*, 951−953.
(25) Sadhukhan, M., and Barman, S. (2013) Bottom-up fabrication of two-dimensional carbon nitride and highly sensitive electrochemical sensors for mercuric ions. *J. Mater. Chem. A 1*, 2752−2756.
(26) Li, Y., Zhao, Y., Cheng, H., Hu, Y., Shi, G., Dai, L., and Qu, L. (2012) Nitrogen-doped graphene quantum dots with oxygen-rich functional groups. *J. Am. Chem. Soc. 134*, 15−18.
(27) Li, X., Zhang, J., Shen, L., Ma, Y., Lei, W., Cui, Q., and Zou, G. (2009) Preparation and characterization of graphitic carbon nitride through pyrolysis of melamine. *Appl. Phys. A: Mater. Sci. Process. 94*, 387−392.
(28) Ma, J., Guo, B., Cao, X., Lin, Y., Yao, B., Li, F., Weng, W., and Huang, L. (2015) One-pot fabrication of hollow cross-linked fluorescent carbon nitride nanoparticles and their application in the detection of mercuric ions. *Talanta 143*, 205−211.
(29) Xu, Y., Niu, X., Zhang, H., Xu, L., Zhao, S., Chen, H., and Chen, X. (2015) Switch-on fluorescence sensing of glutathione in food samples based on a graphitic carbon nitride quantum dot (g-CNQD) − Hg^{2+} chemosensor. *J. Agric. Food Chem. 63*, 1747−1755.
(30) Zhu, J., Xiao, P., Li, H., and Carabineiro, S. A. C. (2014) Graphitic carbon nitride: synthesis, properties and applications in catalysis. *ACS Appl. Mater. Interfaces 6*, 16449−16465.
(31) Song, Z., Lin, T., Lin, L., Lin, S., Fu, F., Wang, X., and Guo, L. (2016) Invisible security ink based on water-soluble graphitic carbon nitride quantum dots. *Angew. Chem., Int. Ed. 55*, 2773−2777.
(32) Cao, X., Ma, J., Lin, Y., Yao, B., Li, F., Weng, W., and Lin, X. A. (2015) Facile microwave-assisted fabrication of fluorescent carbon nitride quantum dots and their application in the detection of mercury ions. *Spectrochim. Acta, Part A 151*, 875−880.
(33) Barman, S., and Sadhukhan, M. (2012) Facile bulk production of highly blue fluorescent graphitic carbon nitride quantum dots and their application as highly selective and sensitive sensors for the detection of mercuric and iodide ions in aqueous media. *J. Mater. Chem. 22*, 21832−21837.
(34) Xiao, D., Yuan, D., He, H., and Lu, J. (2013) Microwave-assisted one-step green synthesis of amino-functionalized fluorescent carbon nitride dots from chitosan. *Luminescence 28*, 612−615.
(35) Tang, Y., Su, Y., Yang, N., Zhang, L., and Lv, Y. (2014) Carbon nitride quantum dots: a novel chemiluminescence system for selective detection of free chlorine in water. *Anal. Chem. 86*, 4528−4535.
(36) Abdolmohammad-Zadeh, H., and Rahimpour, E. (2016) A Novel chemosensor based on graphitic carbon nitride quantum dots and potassium ferricyanide chemiluminescence system for Hg(II) ion detection. *Sens. Actuators, B 225*, 258−266.
(37) Li, H., Shao, F. Q., Huang, H., Feng, J. J., and Wang, A. J. (2016) Eco-friendly and rapid microwave synthesis of green fluorescent graphitic carbon nitride quantum dots for *in vitro* bioimaging. *Sens. Actuators, B 226*, 506−511.
(38) Liu, S., Tian, J., Wang, L., Luo, Y., and Sun, X. (2012) A general strategy for the production of photoluminescent carbon nitride dots from organic amines and their application as novel peroxidase-like catalysts for colorimetric detection of H_2O_2 and glucose. *RSC Adv. 2*, 411−413.
(39) Thomas, A., Fischer, A., Goettmann, F., Antonietti, M., Muller, J.-O., Schlogl, R., and Carlsson, J. M. (2008) Graphitic carbon nitride materials: variation of structure and morphology and their use as metal-free catalysts. *J. Mater. Chem. 18*, 4893−4908.
(40) Xu, M., He, G., Li, Z., He, F., Gao, F., Su, Y., Zhang, L., Yang, Z., and Zhang, Y. (2014) A green heterogeneous synthesis of N-doped carbon dots and their photoluminescence applications in solid and aqueous states. *Nanoscale 6*, 10307−10316.
(41) Zhou, Y., Desserre, A., Sharma, S. K., Li, S., Marksberry, M. H., Chusuei, C. C., Blackwelder, P. L., and Leblanc, R. M. (2017) gel-like carbon dots: characterization and their potential applications. *ChemPhysChem 18*, 890−897.
(42) Li, F., Liu, C., Yang, J., Wang, Z., Liu, W., and Tian, F. (2014) Mg/N double doping strategy to fabricate extremely high luminescent carbon dots for bioimaging. *RSC Adv. 4*, 3201−3205.
(43) Tao, S., Song, Y., Zhu, S., Shao, J., and Yang, B. (2017) A new type of polymer carbon dots with high quantum yield: from synthesis to investigation on fluorescence mechanism. *Polymer 116*, 472−478.
(44) Khan, W. U., Wang, D., Zhang, W., Tang, Z., Ma, X., Ding, X., Du, S., and Wang, Y. (2017) High quantum yield green-emitting carbon dots for Fe (III) detection, biocompatible fluorescent ink and cellular imaging. *Sci. Rep. 7*, 14866.
(45) Hauck, P., Jentys, A., and Lercher, J. A. (2007) Surface chemistry and kinetics of the hydrolysis of isocyanic acid on anatase. *Appl. Catal., B 70*, 91−99.
(46) Shirley, D. A. (1972) High-resolution X-ray photoemission spectrum of the valence bands of gold. *Phys. Rev. B 5*, 4709−4714.
(47) Martinez, M. T., Callejas, M. A., Benito, A. M., Cochet, M., Seeger, T., Anson, A., Schreiber, J., Gordon, C., Marhic, C., Chauvet, O., et al. (2003) Sensitivity of single wall carbon nanotubes to oxidative processing: structural modification, intercalation and functionalization. *Carbon 41*, 2247−2256.
(48) Hontoria-Lucas, C., Lopez-Peinado, A. J., Lopez-Gonzalez, J. D., Rojas-Cervantes, M. L., and Martin-Aranda, R. M. (1995) Study of oxygen-containing groups in a series of graphite oxides: physical and chemical characterization. *Carbon 33*, 1585−1592.
(49) Xing, Y., Li, L., Chusuei, C. C., and Hull, R. V. (2005) Sonochemical oxidation of multiwalled carbon nanotubes. *Langmuir 21*, 4185−4190.
(50) Wagner, C. D., Zatko, D. A., and Raymond, R. H. (1980) Use of the oxygen KLL auger lines in identification of surface chemical states by electron spectroscopy for chemical analysis. *Anal. Chem. 52*, 1445−1451.
(51) López, G. P., Castner, D. G., and Ratner, B. D. (1991) XPS O 1s binding energies for polymers containing hydroxyl, ether, ketone and ester groups. *Surf. Interface Anal. 17*, 267−272.
(52) Kannan, A., Sivanesan, A., Kalaivani, G., Manivel, A., and Sevvel, R. (2016) A Highly selective and simultaneous determination of ascorbic acid, uric acid and nitrite based on a novel poly-N-acetyl-L-methionine (poly-NALM) thin film. *RSC Adv. 6*, 96898−96907.
(53) Lee, T. H., and Rabalais, J. W. (1977) X-ray photoelectron spectra and electronic structure of some diamine compounds. *J. Electron Spectrosc. Relat. Phenom. 11*, 123−127.
(54) Wang, W., Lu, Y.-C., Huang, H., Feng, J.-J., Chen, J.-R., and Wang, A.-J. (2014) Facile synthesis of water-soluble and biocompatible fluorescent nitrogen-doped carbon dots for cell imaging. *Analyst 139*, 1692−1696.
(55) Hendrickson, D. N., Hollander, J. M., and Jolly, W. L. (1969) Nitrogen 1s electron binding energies, correlations with molecular orbital calculated nitrogen charges. *Inorg. Chem. 8*, 2642−2647.
(56) Bharatam, P. V., Moudgil, R., and Kaur, D. (2003) Electron delocalization in isocyanates, formamides and ureas: importance of orbital interactions. *J. Phys. Chem. A 107*, 1627−1634.
(57) Monici, M. (2005) Cell and tissue autofluorescence research and diagnostic applications. *Biotechnol. Annu. Rev. 11*, 227−256.
(58) Leite, T. C., Coelho, R. G., Da Silva, D., Coelho, W. S., Marinho-Carvalho, M. M., and Sola-Penna, M. (2011) Lactate downregulates the glycolytic enzymes hexokinase and phosphofructokinase in diverse tissues from mice. *FEBS Lett. 585*, 92−98.
(59) Perez-Escuredo, J., Dadhich, R. K., Dhup, S., Cacace, A., Van-Hee, V. F., De Saedeleer, C. J., Sboarina, M., Rodriguez, F., Fontenille, M.-J., Brisson, L., et al. (2016) Lactate promotes glutamine uptake and metabolism in oxidative cancer cells. *Cell Cycle 15*, 72−83.
(60) Suzuki, K., Kobayashi, A., Kaneko, S., Takehira, K., Yoshihara, T., Ishida, H., Shiina, Y., Oishi, S., and Tobita, S. (2009) Reevaluation of absolute luminescence quantum yields of standard solutions using a spectrometer with an integrating sphere and a back-thinned CCD detector. *Phys. Chem. Chem. Phys. 11*, 9850−9860.

DOI: 10.1021/acs.bioconjchem.8b00784
Bioconjugate Chem. 2019, 30, 111−123